Journal of Hydrology: Regional Studies 29 (2020) 100683

Contents lists available at ScienceDirect

Journal of Hydrology: Regional Studies

journal homepage: www.elsevier.com/locate/ejrh

A regional-scale conceptual and numerical groundwater flow model in fluvio-glacial sediments for the Milan Metropolitan area (Northern Italy)

Mattia De Caro*, Roberta Perico, Giovanni B. Crosta, Paolo Frattini, Giorgio Volpi

DISAT – Department of Earth and Environmental Sciences, University of Milano Bicocca, Piazza della Scienza, 4, Milan 20126, Italy

ARTICLE INFO

Keywords:
Hydrofacies
Fluvio-glacial sediments
Aquifer parametrization
Regional-groundwater flow

ABSTRACT

Study region: The Milan metropolitan area lies on one of the most important aquifer in Italy, heavily exploited for public and industrial water supply. The area, covering 3135 km^2 in the Po Plain (Northern Italy) with a continental climate, is bounded by the Po, the Adda and the Ticino rivers and by the prealpine foothills. Regional hydrology is characterised by a network of natural and man-made elements, and lowland springs. The sedimentary sequence, from bottom to top, is formed by meandering river plain deposits, the distal fringe of the glacial outwash plains and proximal braid-plain deposits.

Study focus: This study proposes a general approach for aquifer geometry reconstruction and hydrodynamic parametrization of hydrofacies in fluvio-glacial deposits, and their implementation into a 3D regional groundwater flow model. This approach is based on sedimentologically-defined lithofacies/hydrofacies and their correlation in space to obtain nearly homogeneous subunits starting from available data (i.e. 8628 borehole logs, grain size distributions, well tests) and sedimentological knowledge.

New hydrological insights for the region: The calibrated 3D FEM groundwater model allows quantifying the main components of the hydrogeological budget at the regional scale, and the fluxes among the different hydro-stratigraphic units. A sensitivity analysis of groundwater levels to the main recharge components suggests importance of anthropogenic disturbances with respect to natural recharge, and that land-use change may impact water resources more than climate change.

1. Introduction

Most urban areas are located in alluvial plains composed of loose sedimentary deposits where large and highly productive aquifers exist, favouring the settlement of large populations. For example, the Milan Metropolitan area (Northern Italy) hosts about 5 million people, corresponding to 8.5% of the Italian population (ISTAT, 2014). Such urban concentration leads to an increasing pressure on groundwater resources in terms of abstraction and contamination (Goutaland et al., 2013). Intense abstraction from aquifers and changes in land use modify groundwater flow by forcing new discharge and recharge patterns (Foster, 2001). In the last few decades, many cities in the world started experiencing a groundwater rebound as the water demand by the industrial sector has fallen (e.g. Milano, Crosta and De Caro, 2018; Paris, Lamé, 2013; Tokyo, Hayashi et al., 2009; Barcelona, Vázquez-Suñé et al., 2005; Melbourne,

* Corresponding author.
E-mail address: m.decaro@campus.unimib.it (M. De Caro).

https://doi.org/10.1016/j.ejrh.2020.100683
Received 18 July 2019; Received in revised form 4 March 2020; Accepted 13 March 2020
Available online 30 March 2020

Mudd et al., 2004) with consequent concerns about damage to subsurface engineering structures, flooding of subsurface facilities, excessive ingress of groundwater in sewers, chemical attack on concrete foundations, and the mobilization of contaminants (Lelliott et al., 2006; Foster, 2001; Cheney et al., 1999; Heathcote and Crompton, 1997; Greswell et al., 1994; Brassington, 1990).

In densely populated areas, accurate hydrogeological models are needed to obtain a reliable tool for groundwater resources management. This requires a careful and reliable reconstruction of the aquifer geometry and proprieties, which can have a significant control on groundwater simulated flow paths (Christensen et al., 2017). For fluvio-glacial aquifers, understanding the heterogeneity of geological units at different scales plays a key role (de Marsily et al., 2005; Bayer et al., 2011; Refsgaard et al., 2012; Seifert et al., 2012; Kearsey et al., 2015). Approaches developed in the literature to describe fluvio-glacial deposits vary as a function of the available input data and the modelling approach. Input data consist of hard data such as direct lithological and stratigraphic observations made on outcrops, laboratory analysis on field samples, or, especially in urban areas, borehole logs. This hard data may be integrated with soft data including indirect observations produced through geophysical surveys (Ouellon et al., 2008; Mele et al., 2013; Comunian et al., 2016) or remote sensing techniques (Christensen et al., 2017). Starting from this data, the level of heterogeneity description may be different depending on the scale of the problem, the difficulty of validating observation accuracy (Kearsey et al., 2015) and the capability of extracting valuable information from the different data sources (Rajabi et al., 2018).

Regarding the modelling approach, deterministic and stochastic (e.g. multiple-point statistics and the transition probability approach) approaches are the most used (Bianchi et al., 2015). Both allow the creation of numerical models consistent with the geological information and with the conceptual model, despite the existence of problems relative to hydraulic parameterization, in the first approach, and to the smoothing error especially at the regional scale, in the second approach (Watson et al., 2015; Caers, 2000).

In this research, the main aim is to develop a regional-scale conceptual and groundwater flow model, starting from borehole data, grain size distributions, and well tests, in order to analyse the overall groundwater flow behaviour and the main flow budget components. This requires a simple model, which should be able to capture the overall groundwater flow behaviour within the main aquifers, without introducing complex fine-resolution behaviours due to deposit heterogeneity. On the other hand, the conceptual and numerical models, although simple, need to be robust and hydro-stratigraphically sound. Hence, to meet the need of simplicity and robustness, a multi-dimensional approach is proposed and illustrated for the fluvio-glacial deposits of the Milan metropolitan area.

The approach relies on two main steps: (i) the exploitation of the sedimentological knowledge of the area (Regione Lombardia and ENI Agip, 2002; Garzanti et al., 2011; Scardia et al., 2012) to constraint the conceptual model, and (ii) the definition of

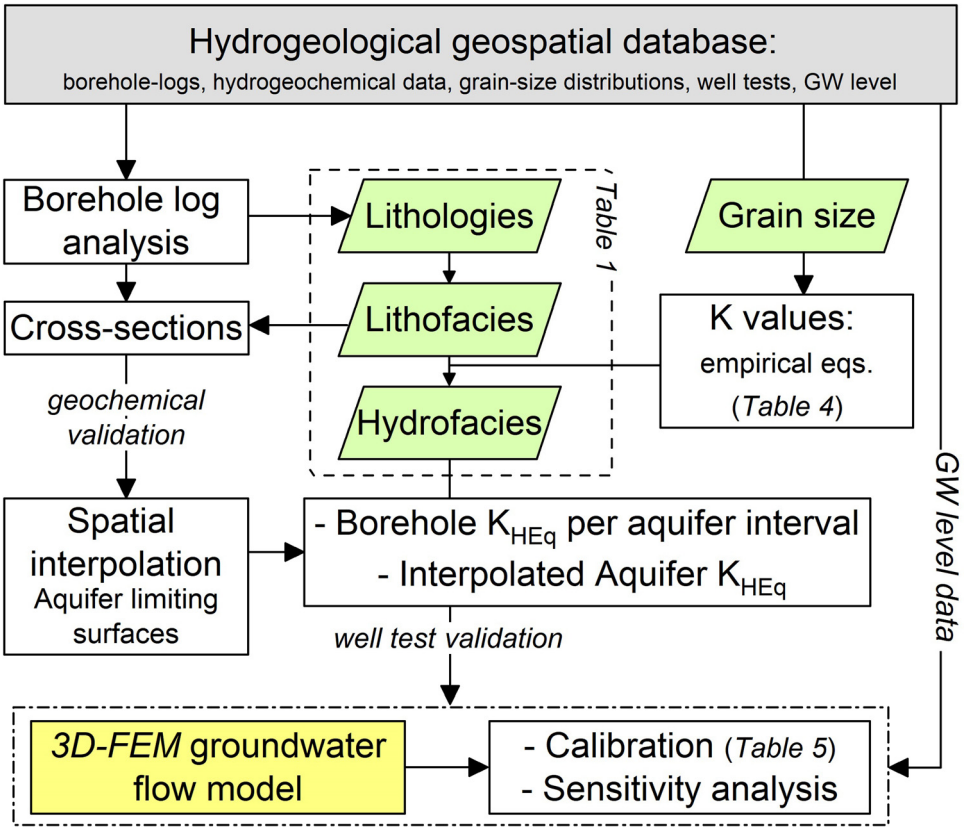

Fig. 1. Conceptual scheme of the proposed approach for the hydrostratigraphic modelling and hydrodynamic parametrization at regional scale.

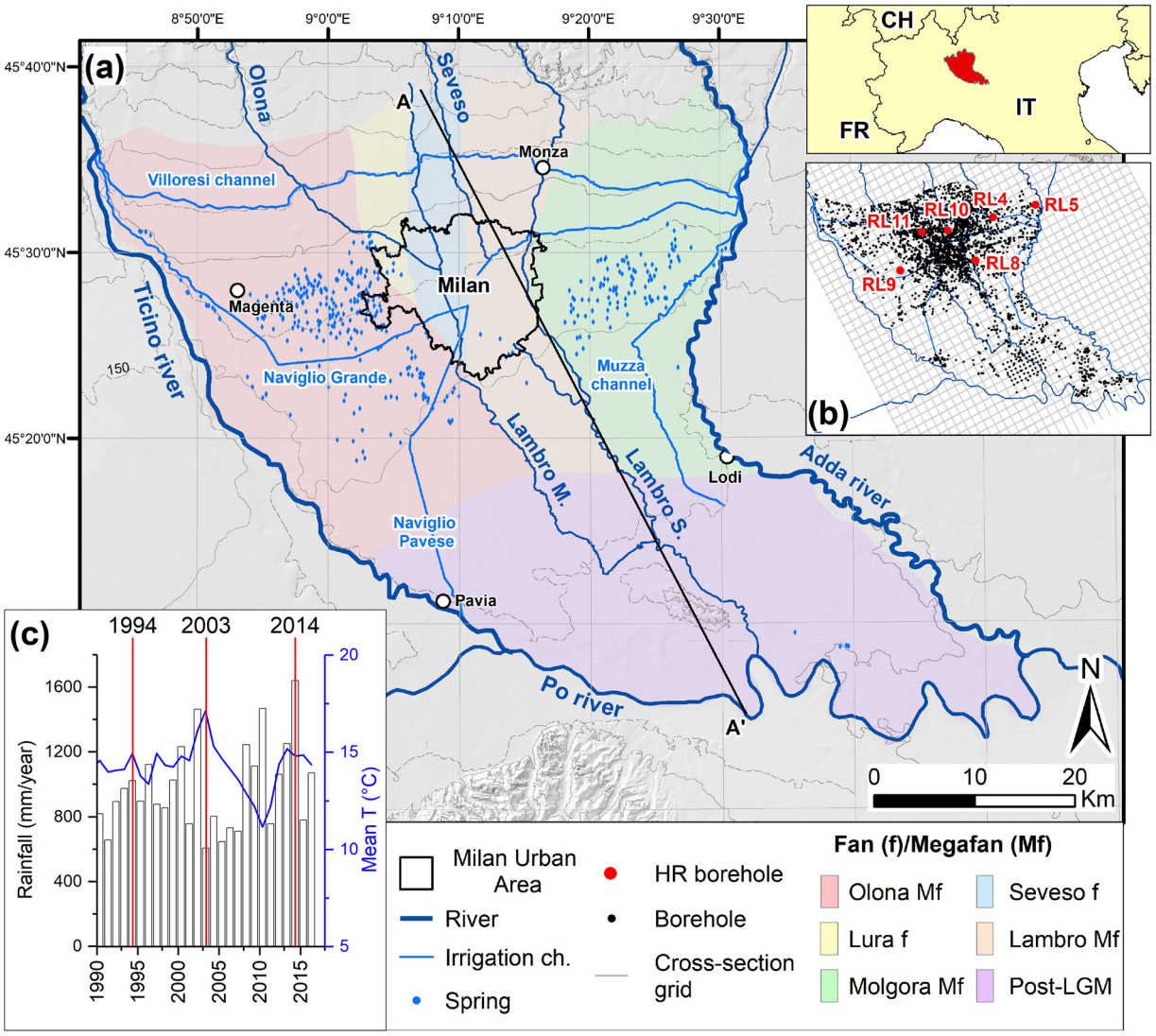

Fig. 2. (a) Map of the study area showing the hydrological network (i.e. rivers, springs and irrigation channels), and the distribution of fan (f) /megafan (Mf) deposits (Fontana et al., 2014); (b) map showing the distributions of boreholes/wells with available stratigraphic/lithologic logs, and the grid of 160 cross-sections. (c) Time series of meteorological data (red lines indicate the considered groundwater flow scenarios).

hydrologically-meaningful hydrofacies units through the analysis of borehole data and grain size distributions to assign hydraulic properties to the aquifers. This approach (Fig. 1) involves: 1) the reconstruction of the aquifer geometry starting from well logs through a novel classification of the lithologies, 2) the interpretation of cross-sections and the interpolation of aquifer boundary surfaces, 3) the definition of hydrofacies for the aquifer parametrization, based on empirical relationships and validated by well test data, and 4) the development of a regional steady-state groundwater flow model to study the major components of the groundwater flow system. For the Milan metropolitan area, several studies have been proposed, which combine geological and geophysical data for the characterisation of the textural variations of the fluvio-glacial deposits different at scales. However, the rigorous recognition of specific sedimentological and stratigraphic sequences, the definition of hydrofacies groups, and the validation by means of available datasets, add meaning and robustness to this work, highlight the difference with previous works in this area (Giudici et al., 2000; Bonomi, 2009; Giudici, 2010; Mele et al., 2012, 2013; Comunian et al., 2016).

2. Study area

The Milan metropolitan area (Fig. 2a) is a portion (3135 km^2) of the Po Plain (Northern Italy) bounded by the Po River to the south, the Adda and the Ticino rivers to the east and west, respectively, and by the Prealps foothills to the north. The climate is continental and the mean annual precipitation ranges from 600 mm/year to over 1400 mm/year from south to north (Fig. 2c)

The study area is located downslope of the frontal moraines at the outlets of the Adda and Ticino Alpine valleys and consists of

glacial terraces and alluvial fan deposits, subdivided in to high, middle and low plains, with a grain size decreasing southward.

The hydrology of the area is characterised by a dense network (Fig. 2a) of natural and man-made elements such as rivers, irrigation channels and lowland springs locally called *Fontanili*. These are man-modified lowland springs (Fig. 2a), observed all over the Po Plain within an E–W trending 20-kilometer-wide belt (about 600-kilometer-long) at the transition between the high and low plains. Along this transition, the groundwater circulating within the coarse-grained sediments rises to the ground level when it meets the fine-grained sediments (Minelli et al., 2001).

Three main depositional sequences have been recognised (Scardia et al., 2006, 2012; Garzanti et al., 2011) which can be summarized as follows (from bottom to top, Fig. 3a):

- The deep confined sequence consists of sandy lenses within clay and silt units representing the lower Pliocene continental-marine facies (*PS1* sequence, late Early Pleistocene, 1.4–0.87 Ma) formed by meandering river plain deposits fed from the Western and Central Alps, and prograding axially in low subsidence settings. The sequence base consists of Pliocene continental-marine deposits.
- The overlying sequence consists of sands and sandy gravels, ranging in thickness between 50 m and 150 m. and corresponds to the distal fringe of the glacial outwash plains which transversally prograde moving southward. The base of the sequence consists of clay and silt layers, and locally of conglomeratic units (locally known as Ceppo) and marks the synchronous and widespread progradation of the braid-plain sequences (*PS2*) over the previous meandering river deposits during the major Pleistocene glaciations in the Alps (about 0.87 Ma).
- The upper sequence consists mainly of gravel with a sandy matrix. This sequence, with a thickness between 20 m and 100 m, overlays a clayey silty layer which is continuous in the southern portion of the study area, but it disappears moving northward. The inferred age of this layer is about 0.45 Ma (Regione Lombardia and ENI Agip, 2002). The sequence (*PS3*) has been developed during the Middle-Late Pleistocene and consists of proximal braid-plain deposits. Recently, the compositional variations of the upper part of this sequence have been related to the *LGM* (Last Glacial Maximum between 22,000- and 16,000-year BP) and post *LGM* evolution of alluvial megafans and fans identified in the study area (Lambro megafan, Seveso fan, Olona megafan, Lura fan, and Molgora megafan) (Fontana et al., 2014) (Fig. 1).

To the south, the Pleistocene-to-Holocene reorganization and entrenchment of the river network led to the latest phase of uplift of the San Colombano hill (Fig. 1) and adjacent areas (Zuffetti et al., 2018).

From a hydrogeological point of view, the three sedimentary sequences correspond to the aquifer groups of the Northern Po Plain, referred in the literature as A (unconfined aquifer corresponding to *PS3*), B (semi-confined aquifer, *PS2*), and C (confined aquifer, *PS1*) (Regione Lombardia and ENI Agip, 2002). The present study focuses on the first two aquifers, A and B.

3. Stratigraphic modeling

In the present study, the hydrostratigraphic model has been delineated by using a multi-dimensional approach (Fig. 1) starting from borehole log analysis (1D), to cross-section interpretation (2D), and spatial interpolation of aquifer limiting surfaces (3D).

3.1. Borehole log analysis

The regional stratigraphic database C*ASPITA* (Regione Lombardia, 2016) collects the borehole logs for the Lombardy-Po Plain area (Fig. 2b). The database contains information regarding the position, the elevation, the depth and the lithological description of the sediments. For the study area, 8628 borehole logs were collected and stored in a georeferenced database (Fig. 2) together with 6 high-resolution borehole logs from Regione Lombardia and ENI Agip (2002).

The 1D analysis consisted of grouping the lithological data according to a hierarchical order (Table 1) based on viable stratigraphic and hydrogeologic rules, and considering the literature existing for small subdomains of the study area (Zappa et al., 2006; Mele et al., 2012; Cavalli, 2012; Comunian et al., 2016). Since the stratigraphic database contains 34,582 unique descriptors, a preliminary analysis has been performed to properly code the information with readily accessible codified lithological descriptions using indices which represent abbreviations for typical features (Bayer et al., 2011). A code ([*i*]*L*) was used, where *L* denotes the prevailing texture (*G* for gravel, *S* for sand, *M* for silt, and *C* for clay) or combinations, and *i* indicates the dominant grain size (*c* for coarse, *m* for medium, and *f* for fine). This allowed to reduce the unique descriptors to 94 lithologies.

The lithologies have been further reclassified into 16 lithofacies, considering only the main grain size and the subordinate components, in order to allow the identification of major sedimentary sequences and to define units with assumed homogeneous hydraulic properties.

3.2. Cross-section interpretation

150 vertical cross-sections were interpreted from 1D data at the lithofacies level (Fig. 1, Table 2) to recognize the unconformities between the three fining-upward depositional sequences (PS1, PS2 and PS3) described by Scardia et al. (2012) along the 6 deep (200 m) high-resolution (HR) boreholes (Regione Lombardia and ENI Agip, 2002) (Fig. 2).

The unconformity L1 between the lower meandering river sequence (*PS1*) and the overlying distal braidplain sequence (*PS2*) is marked by the presence of silty clayey and sandy layers (e.g. *M*, *SC*, *SM*, *C*) of the upper part of *PS1* below the conglomeratic-

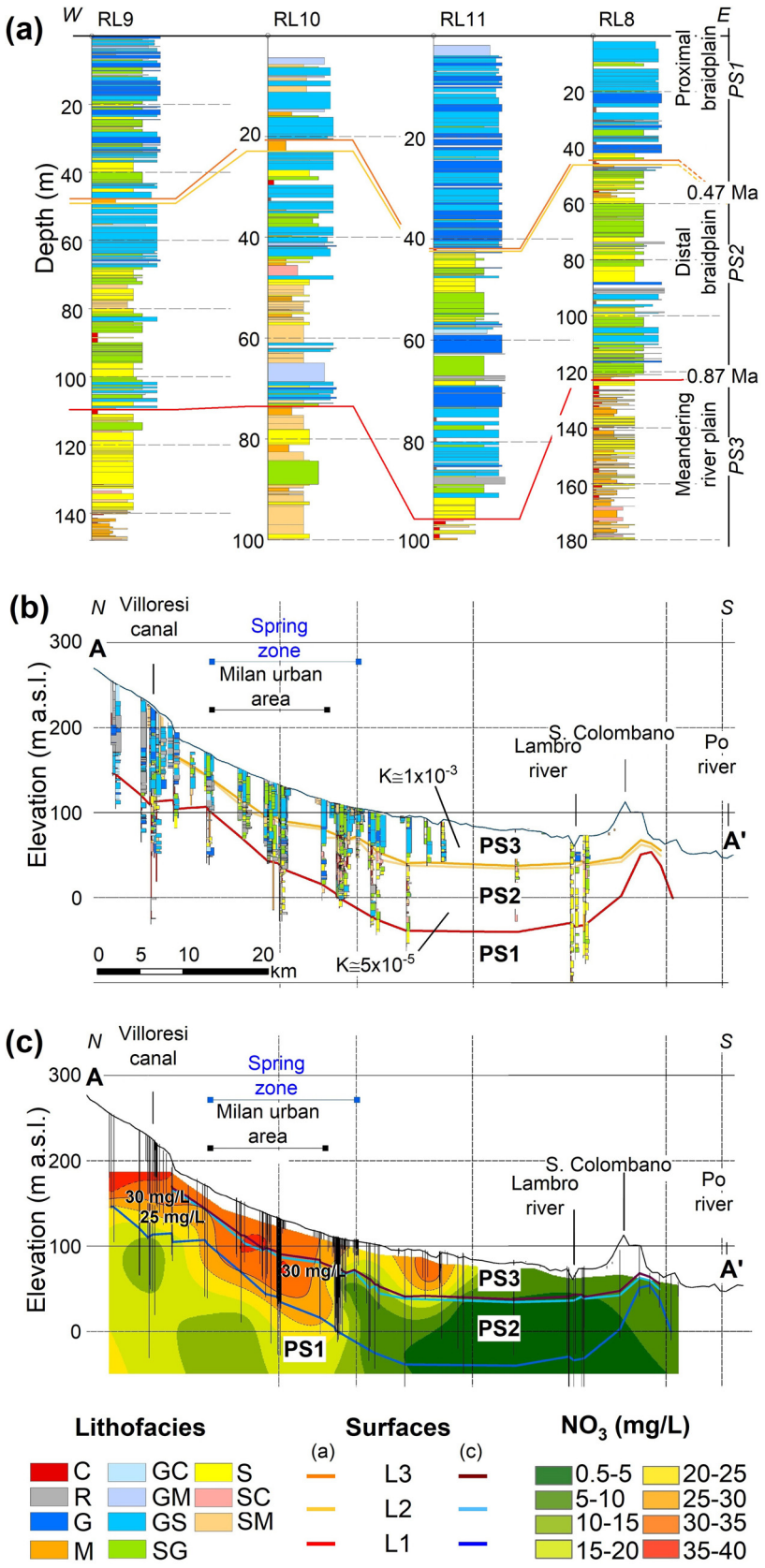

(caption on next page)

Fig. 3. Hydro-stratigraphic reconstruction: (a) example of a N-S cross-section (AA' in Fig. 2) of lithofacies with interpretation of the depositional sequence (PS1, PS2 and PS3) limits, (b) strip-logs of the high resolution (HR)-borehole logs (modified after Scardia et al., 2012) showing the lithofacies vertical distribution, the fining upward sequences and the correlations as proposed by Scardia et al. (2012) (see Fig. 2 for borehole position), and (c) cross-section with aquifer limits and the distribution of nitrate concentration. Labels used in the lithofacies legend are C = clay, M = silt, S = sand, G = gravel, R = rock, and combinations (cfr. Table 1). NO_3 concentration of 25 mg/L is the natural background level (*NBL*) determined via component separation analysis (De Caro et al., 2017).

sandstone (*R*, in the northern sector) or sandy levels (*SG*, *S*) characterizing the bottom of *PS2*. The fining-upward sequence *PS2* shows a clear transition (L2) between coarser deposits (sand and gravels) and sandy, clayey and silty layers (*C*, *M*), the top of which marks the unconformity L3 between *PS2* and the proximal braidplain and megafan sequence (*PS3*), characterized by gravelly layers (*G*, *GS*) in the high plain and sandy layers (S, SG) in the low pain (Fig. 3b).

The concentration of indicator ion species (NO_3, SO_4 and Cl^-) at different depths has been used as a supplemental interpretation criterion (Fig. 3c) in the analysis. In fact, the confined aquifer C (corresponding to PS1) is mostly characterized by natural conditions preserved by the effective separation from the upper aquifers A and B, which are affected by pollution (De Caro et al., 2017). Therefore, the concentrations of main indicator ions associated with anthropogenic pollution delineate the effective separation between the semi-confined and confined aquifers, roughly corresponding to the nitrate natural background level of 25 mg/l (Fig. 3c).

3.3. Spatial interpolation of aquifer limiting surfaces

The elevations of points located on the 2D surface limits (*L1*, *L2*, *L3*) were interpolated to obtain 3D surfaces by using Ordinary Kriging with trend removal and a smoothing factor to adjust the weights of the neighbouring points (Table 3).

For each surface, the interpolation parameters have been optimized on the training subset (i.e. 80% of the points), and validated on a testing subset (i.e. 20% of the points), obtaining root mean square errors of 2.75 m, 3.4 m, and 3.2 m, for *L1*, *L2* and *L3*, respectively.

Table 3 summarizes the parameters that minimize the root-meaN–Square error (E_{RMS}) between interpolated and measured elevations for each surface.

4. Hydraulic parametrization

According to the definition of the aquifer groups given by Regione Lombardia and ENI Agip (2002), the aquifer limiting surfaces included in the stratigraphic model have been assumed to constitute the bottom of the semi-confined aquifer B (*L1*), the bottom of the aquitard between aquifer A and B (*L2*) and the bottom of unconfined aquifer A (*L3*) (see Table 1).

4.1. Hydrofacies definition

Since the lithofacies are defined based on sedimentological criteria, they cannot be easily associated with the hydrological properties of the sediment for the purpose of hydrogeological modelling. This requires the definition of hydrofacies with characteristic permeability and porosity values (Anderson, 1989).

The definition of the hydrofacies and their hydraulic properties is usually based on laboratory data, field measurements, and theoretical calculations on outcrop walls (Kostic et al., 2005; Bayer et al., 2011, 2015). This last approach is unsuitable for our case study where only core logging stratigraphic data, which contain only the description of the prevailing grain size without details about texture or minor structures, are available. Then, a simple approach suitable for core logging data was required.

The grain size distribution of 113 borehole samples (Fig. 4), covering all the sediment-type spectra and different depth intervals in the study area, have been analysed in order to assign tentative hydraulic conductivity (K) values through empirical models, which are based on characteristic values of the grai N-S ize distribution (e.g. the effective diameter d_{10}, the median diameter d_{50}, and the uniformity coefficient C_u), (Supplementary table S1). The most appropriate empirical equations have been selected for each sample based the range of applicability of the methods (Table 4, see also Supplementary table S1). The analysis revealed strong differences within the same lithofacies. Hence, a further subdivision of the lithofacies into subclasses of different hydrofacies with similar hydraulic properties, also accounting for subordinate granulometric components, was required (Table 4). For each hydrofacies, minimum, maximum and mean K values were calculated (Fig. 4, Table 4).

4.2. Hydrodynamic parameter spatialization

Based on the K values of the different hydrofacies, an equivalent depth-averaged K_{eq} for parallel to layer flow conditions was calculated for each borehole of aquifer A (above L3 surface) and B (between L1 and L2 surfaces) by averaging the mean K values of the hydrofacies (Fig. 4 and Table 4) found along the log, weighted by their relative thickness. These K_{eq} values were interpolated, within each aquifer, by the ordinary kriging method to spatialize the single borehole-log hydraulic conductivity value. Fig. 5 shows the computed fields of hydraulic conductivity for the semi-confined (B) and the unconfined (A) aquifers.

In order to evaluate the calculated K_{eq} values, a comparison was made with hydraulic conductivity values obtained by well tests. This comparison was performed by using cumulative probability plots, which display the range of data on a percentile basis and

Table 1
Hierarchical classification of the lithologies obtained through the 1D analysis of 8628 borehole log data and 6 high-resolution stratigraphic logs (Regione Lombardia and Eni, 2002).

	Aquifer and Aquitard/ Aquiclude	Depositional environment	Lithological composition	Lithofacies	Lithologies
Depositional sequence PS3 (Aquifer-A)	Unconfined	proximal braid plain Upper Pliocene	Gravels with sandy matrix, sandy gravels	***G***	*cG,mG,Fg,G, GCong*
				GS	*GS, cGcS, cGmS, cGS, mGS, fGcS,fGmS, fGS, GcS, GmS, GfS, GSC, cmGSM, GSM*
L3	Aquitard	Distal braid plain Middle-Lower Pliocene	Silty layers, silty sands		
				M	*M, MC, MCS, MCG, MG, MS, MSC, MSG*
				SC	*cSC, mSC, fSC, SC, SCG*
				SM	*fSM, mSM, SM, fSMC, SMC, cSMG, cmSMG, mfSMG, fSMG*
L2					
Depositional sequence PS2 (Aquifer-B)	Semi-Confined		Sands, sandy gravels	***GC***	*cGC, GC, GCS*
				GM	*GM*
				S	*S, cS, cmS, mS, mfS, fS*
				SG	*SG, cSG, cmSG, mSG, mfSG, fSG, cSfG, fSfG, ScG, SfG, SGC, cSGM, mSGM, SGM*
				SM	*cSMG, cmSMG, mfSMG, fSMG*
				R	*Ar, ArS, Cong, CongC, CongAr, CongG, CongGC, CongS, CongSC, R*
L1	Aquiclude	Continental-marine transition Lower Pliocene – Miocene	Clayey and silty layers	***C***	*C, CCr, CCong, CcG, CG, CGS, CM, CMG, CMS, CMP, CS, CSG, CSM, CSP, CP*

Alphabetical codification

Prevailing textural codes				Grain size	
G	Gravel	*Cong*	Conglomerate	*c*	Coarse
S	Sand	*M*	Silt	*cm*	coarse-medium
R	Rock	*C*	Clay	*m*	Medium
Ar	Sandstone	*P*	Peat	*mf*	medium-fine
				f	Fine

Table 2
Summary of geometric features of the cross-sections (see. Fig. 2 for the location) interpreted from the recoded borehole log stratigraphies. Spacing and tolerance refer to the distance between cross sections and the maximum distance from a cross-section for a borehole to be considered for the interpretation.

Direction	Number of Cross-sections	Lateral Spacing (m)	Lateral tolerance (m)
NW-SE	38	2500	500
	26	1250	300
E-W	50	2500	500
	46	1250	300

Table 3
Parameters used for the ordinary kriging interpolation of limiting surfaces L1, L2 and L3 (see Table 1).

Surface	L3	L2	L1
Smoothing factor	0.2	0.4	0.2
Nugget (m^2)	5.29	10.17	9.65
Range, *a* (m)	44×10^3	42×10^3	38×10^3
Sill, *c* (m^2)	549.5	604.34	172.73
exponent, d	1.77	1.62	1.89

Trend removal order: 1st order, Searching neighbourhood smooth, semi-variogram type: stable.

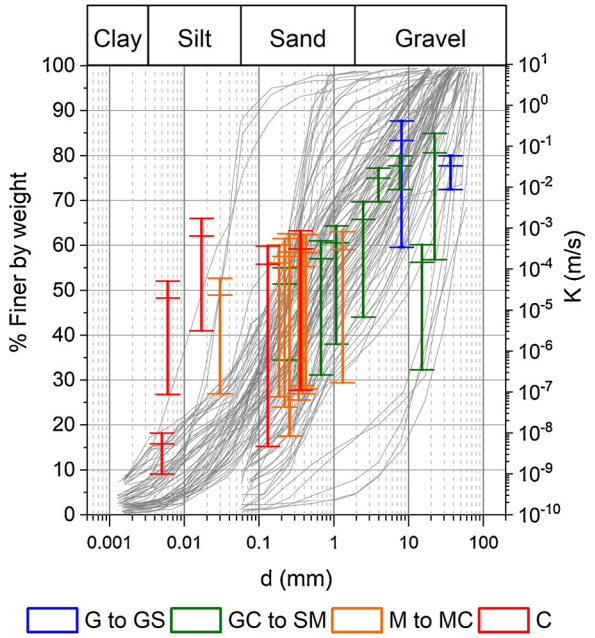

Fig. 4. 113 grain size distributions used for estimating the hydraulic conductivity of lithofacies according to equations in Table 4, and then to define hydrofacies groups; vertical bars show the minimum, the median and the maximum hydraulic conductivity values for each lithofacies of Table 1, and they have been positioned at the d_{50} value.

allows to effectively display and compare the range of data in terms of probability (Edmunds and Shand, 2009). In particular, the comparison was carried out by using different well tests:

- For the unconfined aquifer (A), 21 Lefranc tests (Fig. 5a) have been used, which were made available by the water-distribution companies.
- For the semi-confined aquifer (B), 525 long-term steady-rate pumping tests in the Milan city area (MM S.p.A. historical database) and 68 step-drawdown well tests mainly outside the Milan city area (Fig. 5c) have been used. The transmissivity and the hydraulic conductivity were estimated from these tests by using the Cassan method (1980) and the Theis solution (1935), respectively. These datasets have been considered together since no evident differences have been detected by using the bootstrap method (De Caro, 2018).

Table 4
Lithofacies and hydrofacies with the associated ranges of hydraulic conductivity which account for different samples and different methods applied to each hydrofacies.

Lithofacies	Hydrofacies	Description	K min (m/s)	K mean (m/s)	K max (m/s)	Methods
G	*G*	*Gravel*	8.81×10^{-3}	9.56×10^{-2}	1.82×10^{-1}	(1) (4) (5)
GS	*GS*	*gravel and sand*	1.30×10^{-4}	4.52×10^{-3}	8.92×10^{-3}	(1) (4) (5) (10)
	GSC	*gravel and sand with clay matrix*	6.52×10^{-5}	2.28×10^{-3}	4.49×10^{-3}	(1) (4) (5) (10)
	GSM	*gravel and sand with silt matrix*	3.64×10^{-7}	3.02×10^{-5}	6.01×10^{-5}	(1) (4) (5) (10)
M	*M*	*Silt*	9.01×10^{-8}	3.02×10^{-5}	6.03×10^{-5}	(4) (7)
	MC	*silt and clay*	8.69×10^{-8}	2.57×10^{-5}	5.14×10^{-5}	(4)
	MG	*silt and gravel*	8.36×10^{-8}	2.13×10^{-5}	4.24×10^{-5}	(4)
	MS	*silt and sand*	8.03×10^{-8}	1.68×10^{-5}	3.35×10^{-5}	(4)
SC	*SC*	*sand and clay*	2.63×10^{-7}	3.39×10^{-5}	6.75×10^{-5}	(4) (7) (8) (9)
	SCG	*sand and clay with gravel*	4.46×10^{-7}	5.10×10^{-5}	1.02×10^{-4}	(4) (7) (8) (9)
SM	*SM*	*sand and silt*	6.29×10^{-7}	6.81×10^{-5}	1.35×10^{-4}	(2) (3) (4) (5) (6) (7) (8) (9)
	SMC	*sand and silt with clay*	2.46×10^{-7}	4.43×10^{-6}	8.62×10^{-6}	(2) (3) (4) (5) (6) (7) (8) (9)
	SMG	*sand and silt with gravel*	1.61×10^{-7}	1.80×10^{-5}	3.58×10^{-5}	(2) (3) (4) (5) (6) (7) (8) (9)
GC	*GC*	*gravel and clay*	9.59×10^{-6}	2.56×10^{-3}	5.11×10^{-3}	(2) (3) (4)
GM	*GM*	*gravel and silt*	8.19×10^{-6}	2.39×10^{-3}	4.77×10^{-3}	(2) (3) (4)
S	*S*	*Sand*	1.40×10^{-6}	1.73×10^{-4}	3.45×10^{-4}	(2) (4) (6) (9) (10)
SG	*SG*	*sand and gravel*	6.80×10^{-6}	2.22×10^{-3}	4.42×10^{-3}	(2) (4) (5) (6) (8) (10)
	SGC	*sand and gravel with clay matrix*	3.55×10^{-6}	1.12×10^{-3}	2.24×10^{-3}	(2) (3) (4) (5) (6) (8) (10)
	SGM	*sand and gravel with silt matrix*	3.04×10^{-7}	2.51×10^{-5}	4.99×10^{-5}	(2) (3) (4) (5) (6) (8) (10)
R	*undefined*					
C	*C*	*Clay*	1×10^{-9}	5.5×10^{-9}	1×10^{-8}	(4) (7)
	CG	*clay and gravel*	4.22×10^{-8}	1.06×10^{-5}	2.12×10^{-5}	(4)
	CM	*clay and silt*	1.24×10^{-7}	1.24×10^{-7}	1.24×10^{-7}	(4)
	CS	*clay and sand*	1.32×10^{-7}	1.69×10^{-5}	3.37×10^{-5}	(4)
	CP	*clay and peat*	8.68×10^{-8}	2.57×10^{-5}	5.13×10^{-5}	(4)

Method reference: (1) Alyamani and Şen, 1993, (2) Chapuis et al., 2005, (3) Beyer, 1964, (4) Harleman et al., 1963, (5) Hazen, 1892, (6) Kozeny, 1953, (7) Carman, 1937, (8) NAVFAC, 1974; from Chesnaux et al., 2011, (9) Sauerbrei from Vuković and Soro, 1992, (10) Slichter, 1899.

The comparison of empirical values and well-test results does not reveal relevant differences in terms of probability distribution, thus supporting the reliability of the interpolated K_{eq} values.

4.3. Definition of hydrostratigraphic units

According to their hydrodynamic characteristics, the two main aquifers (A and B) were further subdivided into relatively homogeneous subunits for the purpose of groundwater flow modelling. This spatial discretization can be summarized as follows:

- Within the unconfined aquifer (A), three homogeneous zones have been identified (Fig. 5a): (i) a high-conductivity zone (5×10^{-2} m/s to 5×10^{-3} m/s) consisting of proximal gravelly fan deposits in the northern sector, (ii) a moderate conductivity zone (5×10^{-3} m/s to 1×10^{-4} m/s) characterized by distal sandy fringes of fan deposits in the southern sector of the *fontanili*-belt, and (iii) a low-conductivity zone (1×10^{-4} m/s to 1×10^{-5} m/s) corresponding to post-LGM deposits (as defined in Fontana et al., 2014). Hence, two gentle-slope surfaces (*L4* and *L5,* Fig. 6a) linking the aquitard (base of unconfined aquifer A) to the ground surface (Fig. 6a) were introduced to separate these three zones.
- Within the semi-confined aquifer, two homogeneous zones have been distinguished: (i) a proximal (northern) portion characterized by a larger variability in hydraulic conductivity values (5×10^{-4} m/s to 1×10^{-5} m/s) and (ii) a distal (southern) portion showing quite homogeneous hydraulic conductivity (5×10^{-5} m/s to 1×10^{-5} m/s).

The volumetric distribution of each hydrofacies within each identified subunit (i.e. proximal and distal fan fringes, post-LGM deposits, and proximal and distal semi-confined aquifers) has been analysed (Fig. 6) showing a good agreement with the conceptual stratigraphic model.

5. Groundwater modelling

The hydrostratigraphic model was implemented into a 3D finite element model (FEFLOW; Diersch, 2014) for groundwater modelling (Fig. 6a). A steady-state condition was used to simulate the regional hydraulic head of three years (1994, 2003, and 2014) for which groundwater level data were collected from over 447 monitoring points in the whole Lombardy region (145 in the study area) by the regional management and protection water plan (Regione Lombardia, 2017). In particular, the steady-state model was calibrated for 2014 and successively validated for 1994 and 2003.

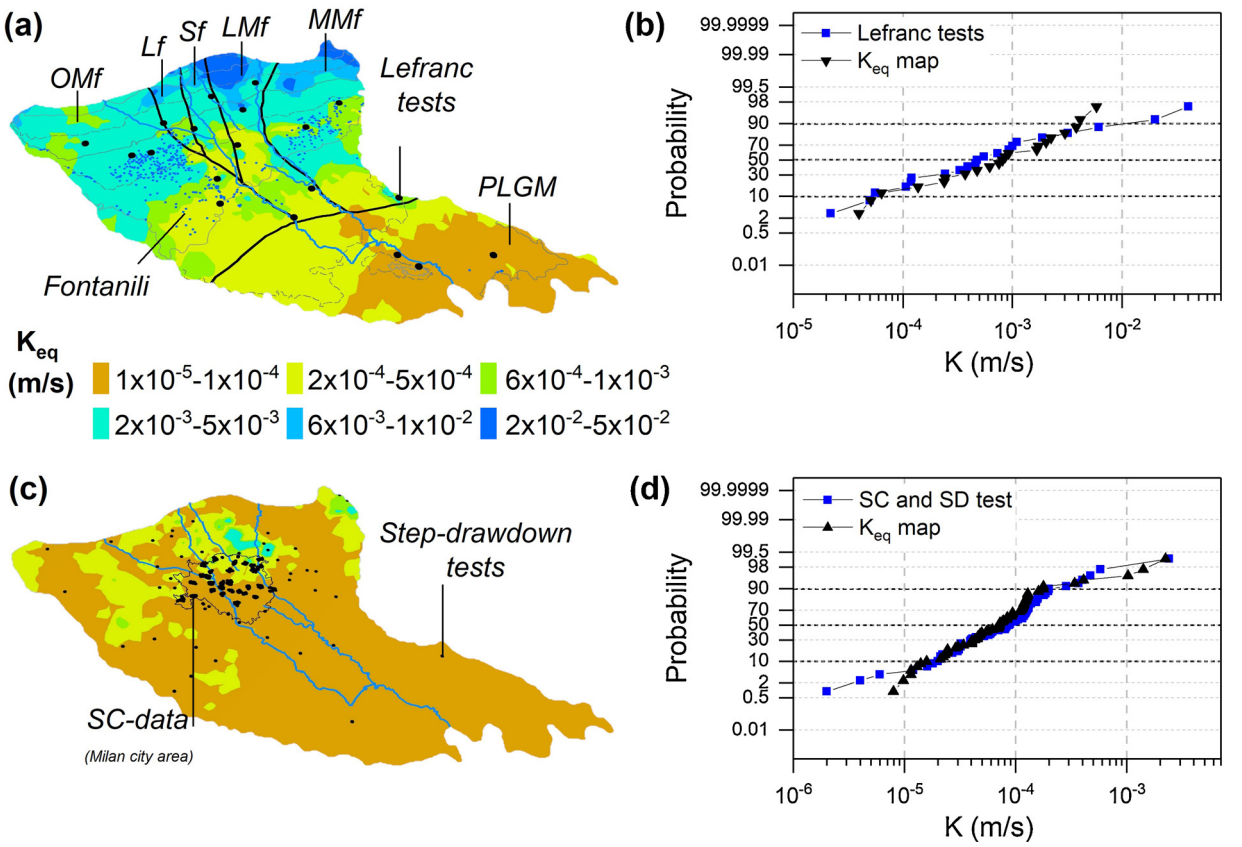

Fig. 5. Results of hydraulic characterization of the analysed aquifers. (a) and (c) are maps of estimated hydraulic conductivity obtained by Ordinary Kriging interpolation for the unconfined aquifer and the semi-confined aquifers, respectively. Black dots in (a) represent the location of available Lefranc tests and labels stay for the fan and megafan subdivision by Fontana et al. (2014). Points in (c) represent the location of well-test (small points) and specific capacity data (big points). (b) Cumulative probability distributions of hydraulic conductivity from Lefranc tests and from interpolated K_{eq} sampled at the same locations of the Lefranc tests (a); (d) cumulative probability distributions for hydraulic conductivity from 68 step-drawdown (SD) tests, 525 specific capacity (SC) data tests and from interpolated K_{eq} sampled at the same well locations.

5.1. Model setup

The 3D finite element model includes 12,040,320 triangular prismatic finite elements divided in to 12 layers (1,003,360 elements per layer):

- Layers 1–4 represent the unconfined aquifer above the *L3* surface (Fig. 6a) with a mean (total) thickness of about 35 m. This aquifer is divided into three hydrostratigraphic units by the L4 and L5 surfaces (Fig. 6a). Moreover, the distal and proximal fan deposits above L5 have been further subdivided into 5 fan and megafan zones (from W to E: Olona megafan, *OMf*; Lura fan, *Lf*; Seveso fan, *Sf*; Lambro megafan, *LMf*, and Molgora megafan, *MMf*, according to Fontana et al., 2014).
- Layer 5 represents the discontinuous aquitard between the unconfined and the semi-confined aquifer, with an average thickness of 3 m.
- Layers 6–11 represent the semi-confined aquifer with a mean thickness of 50 m. This is divided into proximal and distal portions (Fig. 6a).

The thickness of each single layer of the 3D model varies between 3 m and 20 m depending on the thickness of the hydrogeological units and on the well-screen length and position, whereas the distance between nodes ranges from 1500 m down to 10 m near pumping wells and rivers.

5.2. Boundary conditions, abstraction and recharge

The northern boundary of the 3D finite-element models is a 1st Type Boundary Condition (BC), with a constant head value derived by the interpolation of groundwater levels measured in 1994, 2003 and 2014 (Regione Lombardia, 2017). Observed heads along that boundary were 168 ± 1.2 m in 1994, 175 ± 0.8 m in 2003 and 178 ± 0.6 m in 2014.

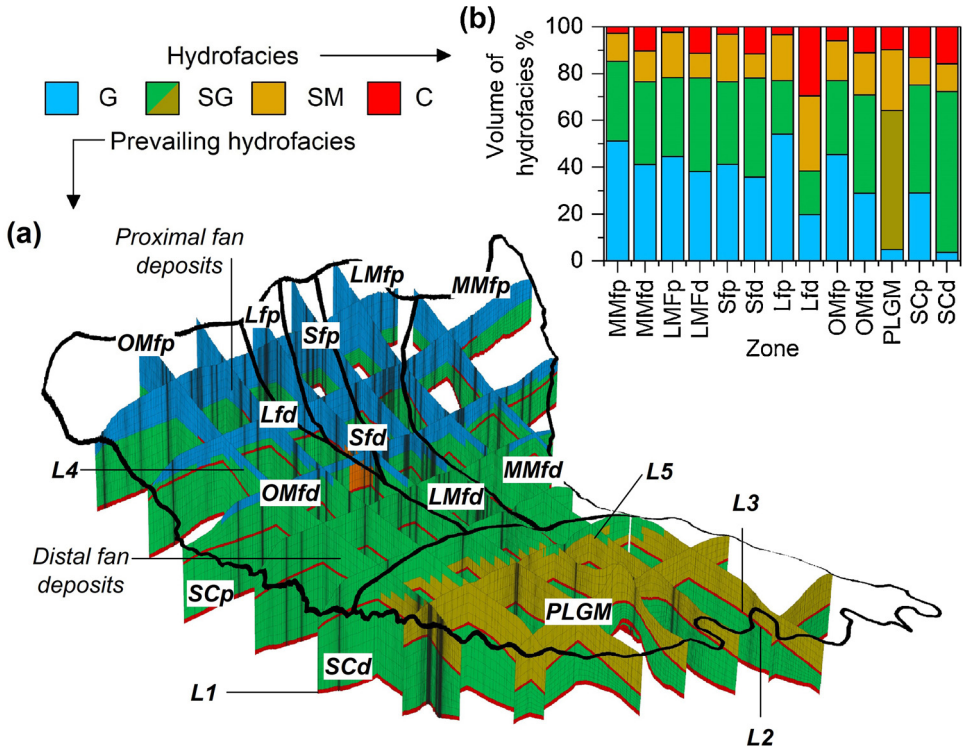

Fig. 6. Spatial discretization of the 3D hydrostratigraphic model: (a) 3D view of the FEM model showing the vertical discretization (by lines L1 and L2) and the prevailing hydrofacies within each sub-unit and, (b) volumetric percentage distribution of each hydrofacies (see Table 1) within each model sub-unit (i.e. fan, megafan, distal and proximal fringes) of the 3D hydrogeological model. Model subunits are OMf = Olona Megafan, Lf = Lura fan, Sf = Seveso fan, LMf = Lambro Megafan, MMf = Molgora Megafan, PLGM = Post-LGM, SC = Semi-confined aquifer, p = proximal (e.g. OMfp), d = distal (e.g. OMfd).

The eastern, western, and southern boundaries are simulated as 1st Type BC, with head values equal to the elevation of the river stage of Adda, Ticino, and Po. These rivers flow at a lower elevation than the regional groundwater level, behaving as gaining rivers. The lowland springs (*Fontanili*) are simulated as seepage faces (i.e. flux-constrained 1st Type BC with hydraulic head equal to the nodal elevation), with a constraint that only allows outflow (Diersch, 2014).

The groundwater abstraction from 1721 wells located in the study area was simulated via the Multi-layer well BC (Diersch, 2014). The pumping rates are available for 576 wells located in the Milan urban area. For these wells, the total abstraction changed from a maximum of about 350×10^6 m^3/year in the middle '70 s to about 2210×10^6 m^3/year at present (from 260×10^6 m^3/year in 1994 to about 224×10^6 m^3/year in 2014), leading to a relevant groundwater rebound (Crosta and De Caro, 2018). For the remaining 1145 wells of the study area, the pumping rate was obtained from the volume of water distributed for drinking purposes for each municipality (ISTAT, 2013, 2016). For these wells, total groundwater abstraction has been approximately constant over the last few decades, equal to 246×10^6 m^3/year (ISTAT, 2016). All the wells in the Milan urban area are screened in the semi-confined aquifer, while the other wells extract water from both the semi-confined and unconfined aquifers.

Average monthly recharge rates for the study area were derived from a simplified Penman-Grindley model (Penman, 1950; Grindley, 1970) and the evapotranspiration (ET_0) was calculated using Thornthwaite's (1980) equation starting from meteorological data (1950–2016) measured at 23 meteorological stations located within the study area (ARPA, 2016). Annual rainfall recharge values were applied on the model surface excluding urban impervious (no-infiltration) areas mapped from available land-use maps (Regione Lombardia, 2003, 2008, 2012). This allowed to take into account the variation of recharge related to the land-use changes in the three simulated years.

Losses from sewer and supply networks were considered within the Milan urban area, giving an additional recharge rate corresponding to 15% of the total water supply, according to estimates from the water suppliers (MM S.p.A).

The annual irrigation recharge values for the Villoresi, the Naviglio Pavese-Grande, and the Muzza areas were estimated by dividing the total distributed water volume by the extent of farming areas and subtracted by the crop evapotranspiration (ET_c). The ET_c was obtained by multiplying the reference evapotranspiration by an average crop coefficient (K_c) according to the prevalent crop types (Allen et al., 1998): maize, cereals and forages (Regione Lombardia, 2012). For the Muzza and the Villoresi areas, an average basal crop coefficient of 0.3 was applied. For the Naviglio Pavese-Grande area a basal crop coefficient of 0.475 was used, since rice is the prevailing crop type (Regione Lombardia, 2012). With these coefficients, annual irrigation recharge values of 464 mm/year, 613 mm/year and 850 mm/year were obtained for the Villoresi, the Muzza and the Pavese-Naviglio Grande irrigation areas, respectively (Fig. 2).

Table 5
Estimated hydraulic conductivity values of unconfined and semi-confined aquifers used as initial values for the groundwater flow model (for subunit locations and extent see Figs. 1 and 5) and calibrated values of hydraulic conductivity and specific storage.

Subunits/Code		Estimated K [m/s]			Calibrated K		
		Min	Mean	Max	K_h [m/s]	K_v [m/s]	S_s [m^{-1}]
Molgora mf - Proximal	*MMfp*	4.72×10^{-4}	6.76×10^{-3}	2.27×10^{-2}	3.35×10^{-2}	1.61×10^{-2}	1.71×10^{-4}
Molgora mf - Distal	*MMfd*	4.88×10^{-5}	1.03×10^{-3}	4.26×10^{-3}	1.41×10^{-3}	5.92×10^{-4}	5.26×10^{-5}
Lambro mf - Proximal	*LMfp*	2.36×10^{-4}	7.66×10^{-3}	2.32×10^{-2}	7.93×10^{-4}	3.65×10^{-4}	3.04×10^{-4}
Lambro mf - Distal	*LMfd*	2.26×10^{-5}	6.03×10^{-4}	7.36×10^{-3}	1.94×10^{-3}	3.69×10^{-4}	1.22×10^{-4}
Seveso f - Proximal	*Sfp*	9.15×10^{-5}	3.95×10^{-3}	1.33×10^{-2}	2.25×10^{-3}	3.15×10^{-4}	5.17×10^{-4}
Seveso f - Distal	*Sfd*	5.87×10^{-5}	5.96×10^{-4}	3.37×10^{-3}	2.48×10^{-3}	3.97×10^{-4}	1.25×10^{-4}
Lura f - Proximal	*Lfp*	4.5×10^{-5}	3.06×10^{-3}	1.31×10^{-2}	3.85×10^{-4}	1.27×10^{-4}	9.54×10^{-5}
Lura f - Distal	*Lfd*	7.8×10^{-5}	6.97×10^{-4}	1.74×10^{-3}	3.36×10^{-3}	9.74×10^{-4}	1.84×10^{-5}
Olona mf - Proximal	*OMfp*	1.22×10^{-4}	2.31×10^{-3}	1.02×10^{-2}	6.70×10^{-3}	3.28×10^{-3}	2.82×10^{-4}
Olona mf - Distal	*OMfd*	6.3×10^{-5}	1.07×10^{-3}	6.35×10^{-3}	1.96×10^{-3}	9.41×10^{-4}	5.70×10^{-4}
Post-LGM	*PLGM*	1.93×10^{-5}	1.37×10^{-4}	7.54×10^{-3}	2.35×10^{-3}	1.08×10^{-3}	5.91×10^{-5}
Aquitard	*Aqt*	8.38×10^{-9}	3.02×10^{-5}	6.03×10^{-5}	8.61×10^{-7}	9.47×10^{-8}	2.56×10^{-3}
Aquiclude	*Aqc*	1.00×10^{-9}	5.50×10^{-9}	1.00×10^{-8}	1.00×10^{-7}	1×10^{-8}	2.03×10^{-2}
Semi-Confined proximal	*SCp*	2.00×10^{-6}	1.33×10^{-4}	2.39×10^{-3}	5.51×10^{-5}	2.64×10^{-5}	9.60×10^{-5}
Semi-Confined distal	*SCd*	1.60×10^{-5}	9.90×10^{-5}	2.84×10^{-4}	7.66×10^{-5}	7.66×10^{-6}	1.61×10^{-4}

5.3. Modelling results

The hydrodynamic parameters of the steady-state model were calibrated on the 2014 groundwater heads, which are the mean values of two measurements taken on May and September 2014 (the average difference between measured groundwater levels is about 0.25 m) in 124 piezometers. Then, the calibrated model was validated on the piezometric levels of 1994 (217 observation points) and 2003 (152 observation points). The steady-state model calibration was performed by inverse procedure (PEST; Doherty et al., 1995) by using the Gauss-Levenberg-Marquardt algorithm (*GLMA*) to iteratively optimize the model parameters to fit to observed data (i.e. observation points). In each iteration process, the *GLMA* adjusts the parameters (i.e. hydraulic conductivity and storativity) in such a way that the objective function is minimized (Doherty, 2016).

The initial values of hydraulic conductivity (Table 5) were obtained by averaging the interpolated K_{eq} values for each model subunit. During the optimization process, the hydraulic conductivity values were adjusted within the maximum and minimum values (± one order of magnitude) of estimated hydraulic conductivity. Furthermore, different values of the anisotropy ratio (K_v/K_h) in the range between 0.1 and 0.5 (Todd, 1980) were tested. The calibrated values of both hydraulic conductivity and specific storage are reported in Table 5.

Scatter plots of differences between observed and computed groundwater levels of steady state models show mean residuals of 2.87 m, 3.23 m and 3.47 m, for 2014, 2003 and 1994, respectively (Fig. 7a, b, and c). Considering the extent of the study area, these results indicate a reasonable agreement between simulated and observed hydraulic heads, with calibrated hydraulic conductivity values that lay within the range of the estimated values (Table 5). On average, calibrated values for unconfined aquifers varied up to 22% (as logarithm) with respect to the initial values; the variation decreased to 5%, 15% and 3% for the aquitard, the aquiclude and the semi-confined aquifer, respectively.

The hydraulic heads and the flow patterns for the unconfined aquifer in 2014, 2003 and 1994 are shown in Fig. 7. These maps show relevant groundwater level differences between 1994 and 2014 in the Milan metropolitan area, where an increase of about 9 m was observed (Fig. 7d).

The hydrogeological budget (Fig. 7e) shows some differences in the three years, due to the different amounts of rainfall. Among these years, 2003 was the driest with an annual rainfall from 605 mm to 512 mm, and 2014 was the wettest, with an annual rainfall from 1639 mm to 1238 mm.

The total recharge for the whole model from precipitation and irrigation ranges from about $0.8 \times 10^9\ m^3$ in 2003 to $2.9 \times 10^9\ m^3$ in 2014, while the upstream inflow from mountain basins ranges from $3.6 \times 10^9\ m^3$ (2003) to $6.7 \times 10^9\ m^3$ (2014). Groundwater outflows are represented by gaining rivers, lowland springs, lateral outflow (excluding rivers), and well abstraction. Estimated lowland springs outflow is about 47 m^3/s, 22.4 m^3/s and 13.5 m^3/s for 2014, 2003 and1994, respectively. These values agree with the 1988–2000 monitored spring outflow rates that range between 10 m^3/s and 25 m^3/s (Bischetti et al., 2012). The estimated outflow rate across the gaining rivers (Lambro, Adda, Ticino and Po river) ranges between $1.13 \times 10^9\ m^3$ (2003) and $2.8 \times 10^9\ m^3$ (2014), indicatively ranging between 1.5% and 3%, 2.7% and 11%, and 1.3% and 5% of the total annual discharge flow of Ticino, Adda and Po rivers, respectively. Groundwater horizontal outflow ranges between $2.5 \times 10^9\ m^3$ (2003) and $5.9 \times 10^9\ m^3$ (2014). Finally, the vertical flow from the unconfined to the semi-confined aquifer ranges between $389 \times 10^6\ m^3$ in 2003 to $413 \times 10^6\ m^3$ in 2014.

The effect of changes in the sink/source values (i.e. rainfall infiltration, irrigation recharge, and groundwater withdrawals) on the calibrated heads was assessed through a sensitivity analysis by changing these values by specific percentages (± 25%, ± 50%, and ± 100% of the initial values).

The results of the sensitivity analysis are shown in Fig. 8 as difference between the calibrated hydraulic heads at the observation

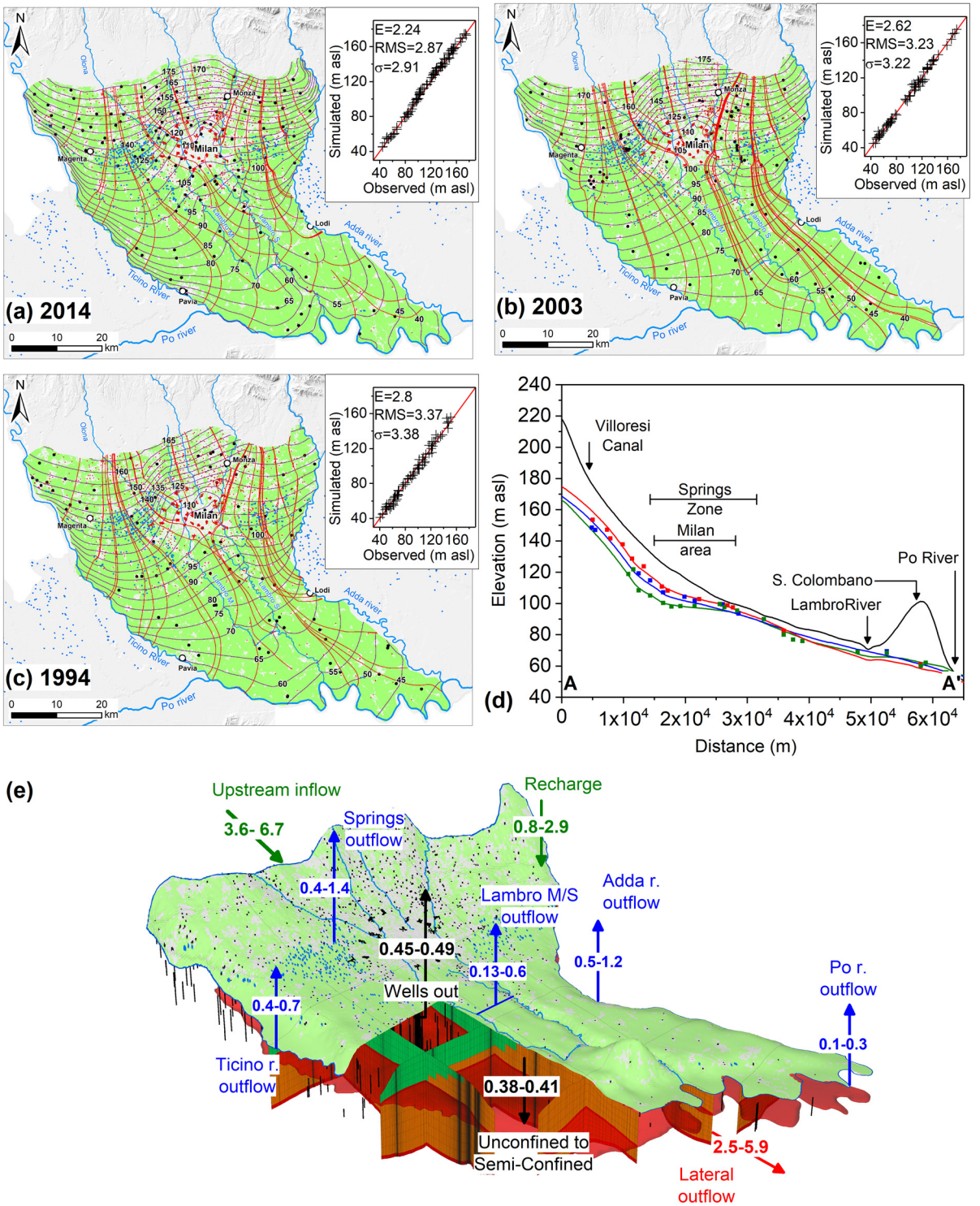

(caption on next page)

Fig. 7. Hydraulic head flow patterns and scatter plots (observed vs. simulated) resulting from steady-state groundwater models for (a) 2014, (b) 2003, and (c) 1994. E, RMS, and σ are the absolute error (in m), the root mean square error (in m), and the standard deviation (in m), respectively. The extent of infiltration areas (i.e. vegetated areas) has been reported for the simulated scenarios (Regione Lombardia, 2003, 2008, 2012). (d) N-S cross-section of simulated steady-state groundwater levels (for section locations see Fig. 2) compared to local observations. (e) Rate-budget scheme for the simulated aquifers showing minimum and maximum inflow, outflow, and aquifer transfer rates. Minimum and maximum values refer to 2003 and 2014, respectively (drought and rainy year).

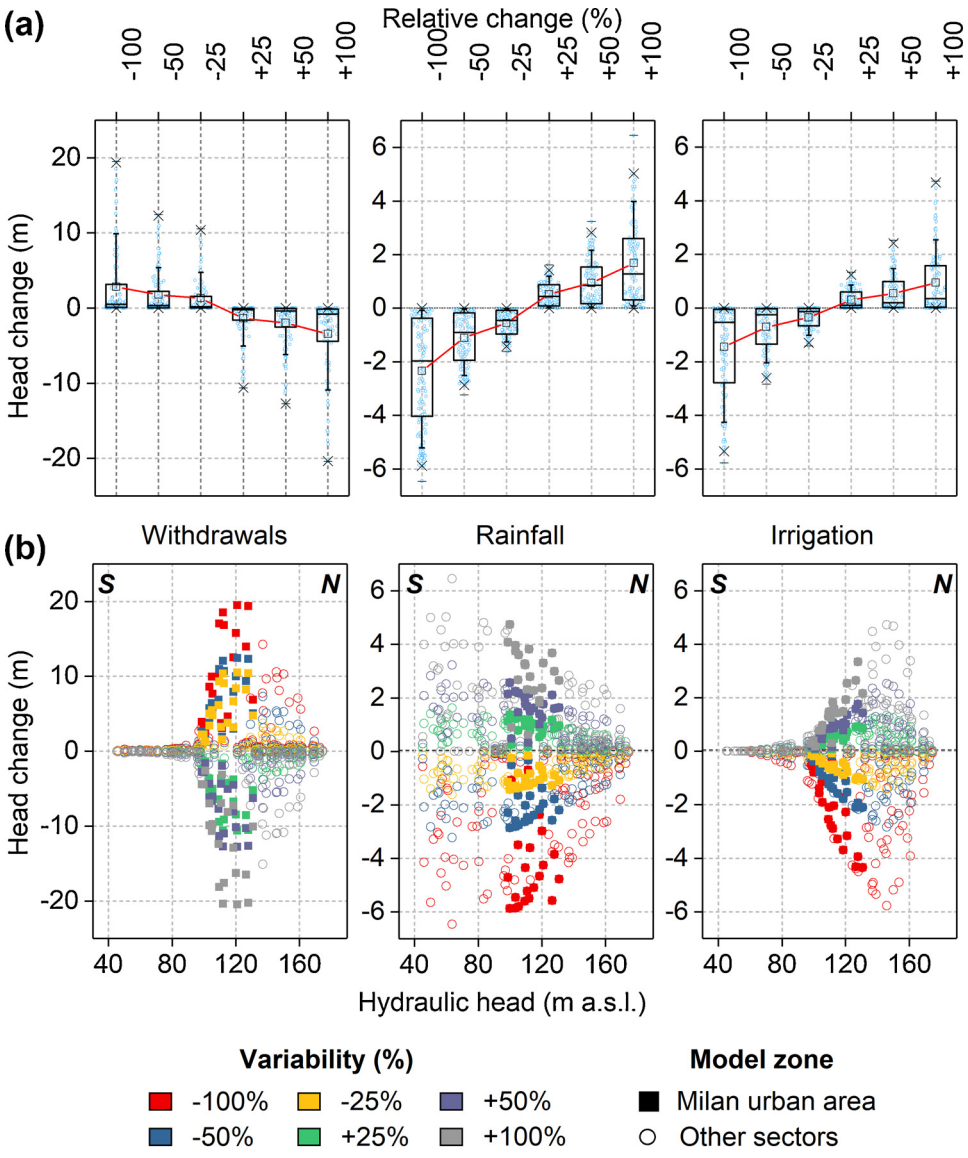

Fig. 8. Sensitivity of groundwater levels to model inputs. (a) Box plot showing the sensitivity to model inputs and (b) scatter plots summarizing the differences (in meters) between calibrated hydraulic heads (i.e. at observation points) and hydraulic heads of sensitivity scenarios. Hydraulic head decreases from N to S.

points and the hydraulic heads of sensitivity scenarios. The groundwater system appears to be sensitive to groundwater abstraction more than to rainfall and irrigation recharge (Fig. 8). A decrease of 25% in groundwater withdrawals leads to a mean head increase in the range between 2 m and 8 m, whereas a decrease of 25% in rainfall and irrigation recharge leads to a mean head decrease in the range between 0.2 m and 2 m (Fig. 8a). The largest influence is computed for the central sectors close to the Milan urban area (around 110 and 125 m a.s.l.; Fig. 8b) whereas almost no change is observed at lower elevations (south of Milano). Rainfall cause the maximum change in areas with lower groundwater depth (south of Milano), whereas irrigation is more effective in the area north sectors where the irrigation channel density is higher.

6. Discussion

6.1. Hydro-stratigraphic modelling and parametrization

For the construction of the conceptual and hydrostratigraphic models, this study fully exploits the available sedimentological knowledge (Regione Lombardia and ENI Agip, 2002; Scardia et al., 2006; Garzanti et al., 2011; Scardia et al., 2012). The deposits of the study area are principally fining upward braid-plain sequences, with aquifers in the coarse deposits at the base of the sequence, and aquitards in the fine deposits of the upper part of the sequence. This conceptual model served as a main criterion for the interpretation of the lithofacies along each borehole, hence, to mark the levels at which transition among the different sequences and aquifers occurs. Moreover, the sedimentological information helped to recognize the different subunits. The upper sequence is characterized by post-LGM fan deposits, which have been subdivided in various upper unconfined aquifer sectors to account for the different clastic facies of proximal and distal fringes of 5 major alluvial fans (Fontana et al., 2014).

The attribution of hydraulic parameters following the qualitative description of single layers, as from the drilling logs, is often affected by a large degree of subjectivity. Therefore, in order to reduce the uncertainty, several empirical relationships based on the grain size distribution parameters, together with well test results, have been used to define hydrofacies groups and to attribute the aquifer properties by isolating homogeneous sediment bodies (Anderson, 1989) characterised by narrow ranges of hydraulic conductivity values. These constitute the initial values of the 3D FEM regional groundwater flow model aimed at the characterization of the groundwater budget components. The possibility to define units with homogeneous hydraulic conductivity is extremely useful because it allows to reduce the computational effort at the expense of a lower resolution in terms of aquifer group heterogeneity. This is strengthened by the fact that the calibrated values of hydraulic conductivity from the groundwater flow model slightly vary with respect to the initial values.

On the other hand, starting from the 16 hydrofacies, it could be possible to develop more complex stratigraphic descriptions by 3D geostatistical methods (i.e. Kriging, Co-Kriging) or by 3D stochastic simulations (i.e. Sequential Gaussian simulation, Sequential Indicator Simulation, Transition Probability on categorical variables such as the hydrofacies; Guadagnini et al., 2004; Zappa et al., 2006; Dell'Arciprete et al., 2012; Comunian et al., 2016), to be used for applications that go beyond the purposes of this research.

6.2. Groundwater models

The hydraulic head distribution (Fig. 7) for the unconfined aquifer suggests that the groundwater level heavily depends on the distance from wells, especially in the highly populated city of Milano, and on gaining rivers at the boundary of the models. The hydrogeological budget shows that the superficial recharge significantly affects the groundwater flow pattern, with total spring and river discharge strongly reduced during dry years (e.g. 2003), and groundwater levels rise leading to higher discharge rates through springs and rivers during rainy years (e.g. 2014, Figs. 7 and 8b). This effect is also evident because the groundwater abstraction, which is the most influential component of the budget according to the sensitivity analysis, is kept constant in the three different years.

The results of the sensitivity analysis on input parameters (i.e. recharge, irrigation, and withdrawals) can be useful to evaluate the potential effects of climate change. An increase of groundwater recharge may result both from wet and cold future scenarios (Allen et al., 2004) due to additional rainfall or from a reduction of evapotranspiration, respectively. On the other hand, a dry scenario with a decrease of recharge might need more irrigation through groundwater withdrawals, which could lower the groundwater levels, or an increase of channel irrigation water volume (i.e. considering the fully-gravity-driven irrigation network) which, in turn, could lead to a groundwater level increase and a decrease in the river stage. A careful investigation of such possible scenarios, which is beyond the scope of this research, will be relevant because it is clearly demonstrated how the sensitivity of groundwater levels to the various inputs is different. For instance, a 50% reduction of withdrawal with respect to the baseline scenario (i.e. 2014) would lead to an increase of the water table up to 10 m in the city of Milan with possible consequences on underground infrastructure. These scenarios should also include the possible decrease in river discharge due to reduced water availability at higher elevation in basins where glaciers are retreating (Aili et al., 2019).

7. Conclusions

Aquifer modelling and prediction of response to perturbations require a reliable representation of sedimentary and hydrogeological processes. In this paper it is demonstrated that a multi-dimensional approach for hydrostratigraphic modelling based on available sedimentological knowledge, together with different methods for estimating aquifer parameters, allows a robust characterization of fluvio-glacial aquifers.

Based on this characterization, a 3D numerical model of the groundwater system was developed and calibrated for the Milan metropolitan area, allowing to quantify the most important components of the regional groundwater system, such as well withdrawals, discharge to gaining rivers and springs, recharge from irrigation networks and vegetated areas and flow transfer between aquifers. Finally, the investigation of the sensitivity of the groundwater system may allow to test hypotheses about the effects of climate and socio-economic changes on the groundwater levels and water budget. For the case study of Milan, for instance, it appears that the impact of climate change may be secondary with respect to anthropogenic stresses, which is an important finding with significant practical implications for a densely populated area such as Milan.

CRediT authorship contribution statement

Mattia De Caro: Conceptualization, Methodology, Writing - original draft. **Roberta Perico:** Data curation, Investigation, Software. **Giovanni B. Crosta:** Supervision, Writing - review & editing. **Paolo Frattini:** Conceptualization, Methodology. **Giorgio Volpi:** Software, Writing - review & editing.

Declaration of Competing Interest

The authors declare that they have no known competing financial interests or personal relationships that could have appeared to influence the work reported in this paper.

Acknowledgments

The authors are deeply indebted to Maurizio Gorla (CAP Holding), Matteo Monti, Marta Gangemi, and Fabio Marelli (MM S.p.a) for providing the original data from the well and step-drawdown tests. The authors are grateful to Andrea Merri, Valeria Marchese, Nicoletta Dotti (ARPA R.L) and Marina Credali for providing the geochemical and groundwater data (PTUA) and the stratigraphic database (CASPITA), respectively. The Consorzio Est Ticino Villoresi is thanked for making available the irrigation discharge data, and Fabio Tradigo (ARUP Italy) for the grain size distribution data.

This article is an outcome of Project MIUR – Dipartimenti di Eccellenza 2018–2022 and PerFORM WATER 2030 project.

Appendix A. Supplementary data

Supplementary material related to this article can be found, in the online version, at doi:https://doi.org/10.1016/j.ejrh.2020.100683.

References

Aili, T., Soncini, A., Bianchi, A., Diolaiuti, G., D'Agata, C., Bocchiola, D., 2019. Assessing water resources under climate change in high-altitude catchments: a methodology and an application in the Italian Alps. Theor. Appl. Climatol. 135 (1-2), 135–156.

Allen, D.M., Mackie, D.C., Wei, M., 2004. Groundwater and climate change: a sensitivity analysis for the Grand Forks aquifer, southern British Columbia, Canada. Hydrogeol. J. 12 (3), 270–290.

Allen, R.G., Pereira, L.S., Raes, D., Smith, M., 1998. Crop evapotranspiration-Guidelines for computing crop water requirements. FAO Irrigation and drainage paper 56. FAO, Rome, 300(9), D05109.

Alyamani, M.S., Şen, Z., 1993. Determination of hydraulic conductivity from complete grain-size distribution curves. Groundwater 31 (4), 551–555.

Anderson, M.P., 1989. Hydrogeologic facies models to delineate large-scale spatial trends in glacial and glaciofluvial sediments. Geol. Soc. Am. Bull. 101 (4), 501–511.

ARPA, Lombardia, 2016. Archivio dati idro-nivo-meteorologici di ARPA Lombardia. Settore monitoraggi ambientali. ARPA Lombardia, Milano (last access: 18 July 2019). http://idro.arpalombardia.it/pmapper-4.0/map.phtml.

Bayer, P., Comunian, A., Höyng, D., Mariethoz, G., 2015. High resolution multi-facies realizations of sedimentary reservoir and aquifer analogs. Sci. Data 2, 150033.

Bianchi, M., Kearsey, T., Kingdon, A., 2015. Integrating deterministic lithostratigraphic models in stochastic realizations of subsurface heterogeneity. Impact on predictions of lithology, hydraulic heads and groundwater fluxes. J. Hydrol. 531, 557–573.

Bayer, P., Huggenberger, P., Renard, P., Comunian, A., 2011. Three-dimensional high resolution fluvio-glacial aquifer analog: part 1: field study. J. Hydrol. (Amst.) 405 (1-2), 1–9.

Beyer, W., 1964. Zur Bestimmung der Wasserdurchlässigkeit von Kiesen und Sanden aus der Kornverteilungskurve. Wasserwirtsch Wassertech 14 (6), 165–168 (In German).

Bischetti, G.B., Fumagalli, N., Piantanida, E.V., Senes, G., Negri, G., Pellitteri, T., Marziali, L., 2012. Tutela e valorizzazione dei fontanili del territorio lombardo. FonTe. 102 p. (In Italian).

Bonomi, T., 2009. Database development and 3D modeling of textural variations in heterogeneous, unconsolidated aquifer media: application to the Milan plain. Comput. Geosci. 35 (1), 134–145.

Brassington, F.C., 1990. Rising groundwater levels in the United Kingdom. Proc. Inst. Civ. Eng. 88 (6), 1037–1057.

Caers, J., 2000. Adding local accuracy to direct sequential simulation. Math. Geol. 32 (7), 815–850.

Carman, P.C., 1937. Fluid flow through granular beds. Trans. Inst. Chem. Eng. 15, 150–166.

Cassan, M., 1980. Les essais d'eau dans la reconnaissance des sols. Eyrolles, France.

Cavalli, E., 2012. Messa a punto di una metodologia per la modellazione tridimesionale e multiscala dell'idrostratigrafia, su base gis. Doctoral dissertation. Università degli Studi di Milano 132 p. (In Italian).

Chapuis, R.P., Dallaire, V., Marcotte, D., Chouteau, M., Acevedo, N., Gagnon, F., 2005. Evaluating the hydraulic conductivity at three different scales within an unconfined sand aquifer at Lachenaie, Quebec. Can. Geotech. J. 42 (4), 1212–1220.

Cheney, C.S., MacDonald, A.M., Forster, A., 1999. Groundwater responses to urbanisation and changing patterns of industrial development in the Wigan metropolitan area, north west England. Int. Contr. Hydrogeol. 21, 111–118.

Chesnaux, R., Baudement, C., Hay, M., 2011. Assessing and comparing the hydraulic properties of granular aquifers on three different scales. Proceedings of Geohydro 2011, Aug. 28–31, Quebec City, Canada, Canadian Quaternary Assoc. and the Canadian Chapter of the International Assoc. of Hydrogeologists 9 p.

Christensen, N.K., Minsley, B.J., Christensen, S., 2017. Generation of 3-D hydrostratigraphic zones from dense airborne electromagnetic data to assess groundwater model prediction error. Water Resour. Res. 53 (2), 1019–1038.

Comunian, A., De Micheli, L., Lazzati, C., Felletti, F., Giacobbo, F., Giudici, M., Bersezio, R., 2016. Hierarchical simulation of aquifer heterogeneity: implications of different simulation settings on solute-transport modeling. Hydrogeol. J. 24 (2), 319–334.

Crosta, G.B., De Caro, M., 2018. Groundwater rebound. In: Bobrowsky, P., Marker, B. (Eds.), Encyclopedia of Engineering Geology. Encyclopedia of Earth Sciences Series. Springer, Cham.

De Caro, M., 2018. Analysis of Groundwater Rebound in the Milan Metropolitan Area by Hydrostratigraphic, Groundwater Quality and Flow Modeling. PhD thesis. University of Milano Bicocca 193. p.

De Caro, M., Crosta, G.B., Frattini, P., 2017. Hydrogeochemical characterization and natural background levels in urbanized areas: milan Metropolitan area (Northern Italy). J. Hydrol. (Amst.) 547, 455–473.

De Marsily, G., Delay, F., Goncalves, J., Renard, P., Teles, V., Violette, S., 2005. Dealing with spatial heterogeneity. Hydrogeol. J. 13 (1), 161–183.

Dell'Arciprete, D., Bersezio, R., Felletti, F., Giudici, M., Comunian, A., Renard, P., 2012. Comparison of three geostatistical methods for hydrofacies simulation: a test on alluvial sediments. Hydrogeol. J. 20 (2), 299–311.
Diersch, H.J., 2014. FEFLOW: Finite Element Modeling of Flow, Mass and Heat Transport in Porous and Fractured Media. Springer-Verlag, Berlin 996 p.
Doherty, J.E., 2016. Model-Independent Parameter Estimation User Manual Part I: Pest Sensan and Global Optimisers. Watermark Numerical Computing, Brisbane, Australia 390 p.
Doherty, J., Brebber, L., Whyte, P., 1995. PEST Model Independent Parameter Estimation, Australian Centre for Tropical Freshwater Research. James Cooke University, Townsville, Australia 140 p.
Edmunds, W.M., Shand, P., 2009. Natural Groundwater Quality. Blackwell Publishing, pp. 1–21 2009.
Fontana, A., Mozzi, P., Marchetti, M., 2014. Alluvial fans and megafans along the southern side of the Alps. Sedimen. Geol. 301, 150–171.
Foster, S.S.D., 2001. The interdependence of groundwater and urbanisation in rapidly developing cities. Urban Water 3 (3), 185–192.
Garzanti, E., Vezzoli, G., Andò, S., 2011. Paleogeographic and paleodrainage changes during Pleistocene glaciations (Po Plain, northern Italy). Earth-Sci. Rev 105 (1), 25–48.
Giudici, M., Foglia, L., Parravicini, G., Ponzini, G., Sincich, B., 2000. A quasi three dimensional model of water flow in the subsurface of Milano (Italy): the stationary flow. Hydrol. Earth Syst. Sci. Discuss. 4 (1), 113–124.
Giudici, M., 2010. Modeling water flow and solute transport in alluvial sediments: scaling and hydrostratigraphy from the hydrological point of view. Proceedings of the Second National Workshop "Multidisciplinary approach for porous aquifer characterization'. In: In: Bersezio, R., Amanti, M. (Eds.), Memorie descrittive della Carta Geologica d'Italia Vol. 90. pp. 113–119.
Goutaland, D., Winiarski, T., Lassabatere, L., Dubé, J.S., Angulo-Jaramillo, R., 2013. Sedimentary and hydraulic characterization of a heterogeneous glaciofluvial deposit: application to the modeling of unsaturated flow. Eng. Geol. 166, 127–139.
Greswell, R.B., Lloyd, J.W., Lerner, D.N., Knipe, C.V., 1994. Rising groundwater in the Birmingham area. In: Groundwater Problems in Urban Areas: Proceedings of the International Conference Organized by the Institution of Civil Engineers and Held in London. 2–3 June 1993, Thomas Telford Publishing. pp. 330–341.
Grindley, J., 1970. Estimation and mapping of evaporation. IAHS Publication (1), 200–213.
Guadagnini, L., Guadagnini, A., Tartakovsky, D.M., 2004. Probabilistic reconstruction of geologic facies. J. Hydrol. 294 (1), 57–67.
Harleman, D.R., Mehlhorn, P.F., Rumer, R.R., 1963. Dispersion-permeability correlation in porous media. J. Hydraul. Div. 89 (2), 67–85.
Hayashi, T., Tokunaga, T., Aichi, M., Shimada, J., Taniguchi, M., 2009. Effects of human activities and urbanization on groundwater environments: an example from the aquifer system of Tokyo and the surrounding area. Sci. Total Environ. 407 (9), 3165–3172.
Hazen, A., 1892. Some Physical Properties of Sands and Gravels, With Special Reference to Their Use in Filtration. Massachusetts State Board of Health, pp. 539–556 24th Annual report.
Heathcote, J.A., Crompton, D.M., 1997. Managing the impact of urban groundwater rise. In: Groundwater in the Urban Environment: Problems, Processes and Management. International Association of Hydrogeologists XXVII Congress. pp. 597–602.
ISTAT, 2016. Water Consumption by Domestic Use: Environmental Data Collection in the City in 2016. Istituto Nazionale di Statistica, Roma (last access: 18 July 2019). http://dati.istat.it.
ISTAT, 2014. Demographic Statistics: Annual Survey on Movement and Calculation of the Resident Population. Istituto Nazionale di Statistica, Roma (last access: 18 July 2019). http://dati.istat.it.
ISTAT, 2013. Urban Water Census: Annual Survey on Water Abstraction for Drinkable Use. Istituto Nazionale di Statistica, Roma (last access: 18 July 2019). http://dati.istat.it.
Kearsey, T., Williams, J., Finlayson, A., Williamson, P., Dobbs, M., Marchant, B., et al., 2015. Testing the application and limitation of stochastic simulations to predict the lithology of glacial and fluvial deposits in Central Glasgow, UK. Eng. Geol. 187, 98–112.
Kostic, B., Becht, A., Aigner, T., 2005. 3-D sedimentary architecture of a Quaternary gravel delta (SW-Germany): implications for hydrostratigraphy. Sediment. Geol. 181 (3-4), 147–171.
Kozeny, J., 1953. Das wasser in boden, grundwasserbewegung. Hydraulik 280–445.
Lamé, A., 2013. Modélisation hydrogéologique des aquifères de Paris et impacts des aménagements du sous-sol sur les écoulements souterrains. Doctoral dissertation. Ecole Nationale Supérieure des Mines de Paris In French.
Lelliott, M.R., Bridge, D.M., Kessler, H., Price, S.J., Seymour, K.J., 2006. The application of 3D geological modeling to aquifer recharge assessments in an urban environment. Quat. J. Eng. Geol. Hydrogeol. 39 (3), 293–302.
Mele, M., Bersezio, R., Giudici, M., Inzoli, S., Cavalli, E., Zaja, A., 2013. Resistivity imaging of Pleistocene alluvial aquifers in a contractional tectonic setting: a case history from the Po plain (Northern Italy). J. Appl. Geophys. 93, 114–126.
Mele, M., Bersezio, R., Giudici, M., 2012. Hydrogeophysical imaging of alluvial aquifers: electrostratigraphic units in the quaternary Po alluvial plain (Italy). Int. J. Earth Sci. 101 (7), 2005–2025.
Minelli, A., Ruffo, S., Stoch, F., Cosentino, A., La Posta, A., Morandini, C., Solari, M., 2001. Risorgive e fontanili. Acque sorgenti di pianura dell'Italia Settentrionale. Quaderni habitat, Ministero dell'Ambiente, Museo Friulano di Storia Naturale, Udine 82 p.
Mudd, G.M., Deletic, A., Fletcher, T.D., Wendelborn, A., 2004. A review of urban groundwater in Melbourne: considerations for WSUD. WSUD 2004: Cities as Catchments; International Conference on Water Sensitive Urban Design, Proceedings of Engineers Australia 248 p.
Navfac, D.M., 1974. Design Manual-Soil Mechanics, Foundations, and Earth Structures. US Government Printing Office, Washington, DC.
Ouellon, T., Lefebvre, R., Marcotte, D., Boutin, A., Blais, V., Parent, M., 2008. Hydraulic conductivity heterogeneity of a local deltaic aquifer system from the kriged 3D distribution of hydrofacies from borehole logs, Valcartier, Canada. J. Hydrol. 351 (1-2), 71–86.
Penman, H.L., 1950. The dependence of transpiration on weather and soil conditions. Eur. J. Soil Sci. 1 (1), 74–89.
Rajabi, M.M., Ataie-Ashtiani, B., Simmons, C.T., 2018. Model-data interaction in groundwater studies: review of methods, applications and future directions. J. Hydrol. 567, 457–477.
Refsgaard, J.C., Christensen, S., Sonnenborg, T.O., Seifert, D., Højberg, A.L., Troldborg, L., 2012. Review of strategies for handling geological uncertainty in groundwater flow and transport modeling. Adv. Water Resour. 36, 36–50.
Regione Lombardia, 2017. Programma di Tutela ed Uso delle Acque della Regione Lombardia PTUA 2016. D.g.r. 31/06/2017 - n. X/6990. .
Regione Lombardia, 2016. Banca dati geologica sottosuolo, Campioni Analisi Sondaggi Penetrometrie e Indagini Territoriali Ambientali (CASPITA). (last access: 18 July 2019). http://www.geoportale.regione.lombardia.it.
Regione Lombardia, 2012. DUSAF 4.0. Destinazione d'uso dei suoli agricoli e forestali 2012. Tech rep. Regione Lombardia, Milano (In Italian).
Regione Lombardia, 2008. DUSAF 2.0. Destinazione d'uso dei suoli agricoli e forestali 2005-2007. Tech rep. Regione Lombardia, Milano (In Italian).
Regione Lombardia, 2003. DUSAF 1.1. Destinazione d'uso dei suoli agricoli e forestali 1999-2000. Tech rep. Regione Lombardia, Milano (In Italian).
Regione Lombardia, Agip, E.N.I., 2002. Geologia degli acquiferi padani della Regione Lombardia. SELCA, Firenze (In Italian).
Scardia, G., De Franco, R., Muttoni, G., Rogledi, S., Caielli, G., Carcano, C., Piccin, A., 2012. Stratigraphic evidence of a Middle Pleistocene climate-driven flexural uplift in the Alps. Tectonics 31 (6).
Scardia, G., Muttoni, G., Sciunnach, D., 2006. Subsurface magnetostratigraphy of Pleistocene sediments from the Po Plain (Italy): constraints on rates of sedimentation and rock uplift. Geol. Soc. Am. Bull. 118 (11-12), 1299–1312.
Seifert, D., Sonnenborg, T.O., Refsgaard, J.C., Højberg, A.L., Troldborg, L., 2012. Assessment of hydrological model predictive ability given multiple conceptual geological models. Water Resour. Res. 48 (6).
Slichter, C.S., 1899. Theoretical investigation of the motion of ground waters. The 19th Ann. Rep. US Geophys Survey 304–319.
Theis, C.V., 1935. The relation between the lowering of the Piezometric surface and the rate and duration of discharge of a well using ground-water storage. EOS Trans. Am. Geophys. Union 16 (2), 519–524.
Thornthwaite, C.W., 1980. An approach toward a rational classification of climate. Geogr. Rev. 38 (1), 55–94 1948.
Todd, D.K., 1980. Groundwater Hydrology, 2nd ed. John Wiley & Sons, New York, pp. 535p.

Vázquez-Suñé, E., Sánchez-Vila, X., Carrera, J., 2005. Introductory review of specific factors influencing urban groundwater, an emerging branch of hydrogeology, with reference to Barcelona, Spain. Hydrogeol. J. 13 (3), 522–533.
Vuković, M., Soro, A., 1992. Determination of Hydraulic Conductivity of Porous Media From Grain-Size Composition. Water Resources Publications, Littleton, Colorado.
Watson, C., Richardson, J., Wood, B., Jackson, C., Hughes, A., 2015. Improving geological and process model integration through TIN to 3D grid conversion. Comput. Geosci. 82, 45–54.
Zappa, G., Bersezio, R., Felletti, F., Giudici, M., 2006. Modeling heterogeneity of gravel-sand, braided stream, alluvial aquifers at the facies scale. J. Hydrol. 325 (1), 134–153.
Zuffetti, C., Bersezio, R., Contini, D., Petrizzo, M.R., 2018. Geology of the San Colombano hill, a Quaternary isolated tectonic relief in the Po Plain of Lombardy (Northern Italy). J. Maps 14 (2), 199–211.